Chinese Journal of
POLYMER SCIENCE

RESEARCH ARTICLE

https://doi.org/10.1007/s10118-026-3737-z
Chinese J. Polym. Sci.

Zinc Ferrite as an Eco-friendly Synergist for Decabromodiphenyl Ethane in Acrylonitrile Butadiene Styrene: an Effective Alternative to Antimony Trioxide for Enhanced Flame Retardancy

Ge-Hao Guo[a,†], Miao-Miao Tian[a,†], Meng-Yuan Zheng[a], Qing-Hua Peng[a], Xiang Tan[b], Chang-Hui Luo[b], Jun Sun[a,c*], Xiao-Yu Gu[a,c], Hong-Fei Li[a,c], and Sheng Zhang[a,c*]

[a] *State Key Laboratory of Organic-Inorganic Composites, Beijing University of Chemical Technology, Beijing 100029, China*
[b] *College of Materials Science and Engineering, Beijing University of Chemical Technology, Beijing 100029, China*
[c] *Beijing Key Laboratory of Advanced Functional Polymer Composites, Beijing University of Chemical Technology, Beijing 100029, China*

Abstract Acrylonitrile butadiene styrene (ABS) is widely used owing to its excellent mechanical properties, thermal stability, and processability; however, its poor inherent flame retardancy limits its applications, which require higher safety. Conventional flame-retardant ABS systems mainly rely on a bromine-antimony synergistic system, in which antimony trioxide (ATO) is costly and environmentally concerning. In this study, decabromodiphenylethane (DBDPE) and ATO were first selected as the flame-retardant systems and combined at a mass ratio of 3:1. The results showed that the ABS/12DBDPE/4ATO composite achieved a UL-94 V-0 rating with a limiting oxygen index (LOI) of 24.0%. Subsequently, zinc ferrite (ZF) nanoparticles were synthesized *via* a co-precipitation method and employed as partial substitutes for ATO in ABS composites. When 50 wt% ATO was replaced by ZF, the ABS/12DBDPE/2ATO/2ZF composite exhibited an increased LOI value of 26.9%, while still achieving a UL-94 V-0 rating. Compared with neat ABS, the peak heat release rate (PHRR) and total heat release (THR) were reduced by 62.1% and 46.3%, respectively. Furthermore, incorporating 5 wt% nitrile butadiene rubber (NBR) significantly improved the toughness of the composite, increasing the impact strength from 3.8 kJ/m^2 to 13.2 kJ/m^2, without compromising flame retardancy. Overall, this study demonstrates an effective and practical strategy to reduce ATO usage while simultaneously enhancing the fire safety and mechanical performance of ABS.

Keywords Acrylonitrile butadiene styrene (ABS); Flame retardancy; Zinc ferrite; Antimony trioxide; Substitution

Citation: Guo, G. H.; Tian, M. M.; Zheng, M. Y.; Peng, Q. H.; Tan, X.; Luo, C. H.; Sun, J.; Gu, X. Y.; Li, H. F.; Zhang, S. Zinc ferrite as an eco-friendly synergist for decabromodiphenyl ethane in acrylonitrile butadiene styrene: an effective alternative to antimony trioxide for enhanced flame retardancy. *Chinese J. Polym. Sci.* https://doi.org/10.1007/s10118-026-3737-z

INTRODUCTION

Acrylonitrile butadiene styrene (ABS) is a widely used thermoplastic engineering plastic known for its excellent comprehensive properties. ABS has been extensively applied in electronic appliances, automotive interior components, and building materials, owing to its favorable thermal stability, mechanical performance, and processing fluidity.[1–5] These properties originate from the synergistic contributions of its constituent phases: acrylonitrile imparts chemical resistance and thermal stability; butadiene provides toughness and impact resistance; and styrene enhances processability and surface gloss.[6–11] However, ABS resins are inherently flammable and release large amounts of toxic fumes during combustion, posing significant risks to human health and safety. Consequently, the development of effective flame-retardant modification strategies is essential to ensure safe and sustainable application of ABS materials.[12–15]

Over the past several decades, halogenated flame retardants used in combination with antimony trioxide (ATO) have been widely adopted to impart flame retardancy to ABS because they deliver a high efficiency at relatively low loadings.[16] This effectiveness principally stems from the synergistic action: Sb species react with Br retardants to produce volatile $SbBr_3$, which enhances the gas-phase flame inhibition mechanism.[17,18] However, ATO has been associated with potential carcinogenic hazards, and $SbBr_3$ formed during combustion exhibits persistent toxicity in aquatic organisms.[19–21] At the same time, dwindling antimony reserves and increasingly stringent environmental regulations have driven the market price of ATO sharply upward, imposing a substantial economic burden on industrial production.

Owing to the mounting health, environmental, and economic concerns surrounding ATO, the development of effective substitutes has attracted considerable attention. Promising candidates include bismuth trioxide (Bi_2O_3), zinc borate (ZB), and various tin compounds. For instance, Zhang *et al.*[22]

* Corresponding authors, E-mail: sunj@mail.buct.edu.cn (J.S.)
E-mail: zhangsheng@mail.buct.edu.cn (S.Z.)
† These authors contributed equally to this work.
Received April 13, 2026; Accepted May 5, 2026; Published online July 22, 2026

reported that incorporating 6 phr Bi_2O_3 into flexible PVC (fPVC) reduced the horizontal burning rate by 20.5% compared to the 4 phr Sb_2O_3/fPVC, achieving complete replacement of Sb_2O_3. This indicates that Bi_2O_3 as an effective antimony free synergist. Additionally, tin- and zinc-based compounds have been widely explored as potential synergists to replace ATO. Zhang *et al.*[23] reported that partially replacing ATO (50 wt%) with ZB or SnO_2 in fPVC reduced the peak release rate (PHRR) by 32.1% and 27.0%, respectively, compared to the $4Sb_2O_3$/fPVC. These findings demonstrate that zinc- and tin-based synergists can effectively enhance the flame-retardant performance when used to partially replace ATO.

However, these commonly used flame retardants often compromise the mechanical properties of the polymer, resulting in reduced toughness and insufficient impact resistance of ABS, rendering it susceptible to stress cracking in practical applications. This degradation principally arises because the flame-retardant particles disrupt the continuous dispersion of the rubber phase within the matrix, creating stress concentrators that promote crack initiation and propagation. Therefore, implementing toughening modifications that preserve or enhance the ABS mechanical performance while achieving flame retardancy is of critical importance. Zhou *et al.*[6] constructed a core-shell flame retardant ADP@SiR (silicone rubber-encapsulated aluminum diethylphosphinate) and incorporated it into ABS. The 20 wt% ADP@SiR/ABS composte exhibited a 433% higher impact strength compared to 20ADP/ABS. Nguyen *et al.*[24] employed nitrile butadiene rubber (NBR) as a toughening agent to enhance the impact resistance of recycled ABS (re-ABS). The impact strength of the blends increased and reached a maximum value of 52.7 kJ/m^2 at a NBR of 10 wt% when compared to neat re-ABS (34 kJ/m^2). Among various elastomers, NBR has attracted extensive attention owing to its excellent compatibility with ABS, outstanding oil resistance, good thermal stability, and high toughness. The polar nitrile groups in NBR can enhance the interfacial adhesion with the ABS matrix, leading to a finely dispersed rubber phase and significantly improved toughness.

In this study, a ferrite-based additive exhibiting high flame-retardant efficiency, resource abundance, and low cost was prepared by solution co-precipitation followed by calcination and evaluated as an alternative to conventional antimony trioxide in ABS flame-retardant formulations. Concurrently, NBR was incorporated to toughen the ABS matrix, with the goal of synergistically improving impact resistance and flame retardancy. The results demonstrated a viable strategy for producing ABS composites that combine effective flame protection, enhanced toughness, and improved environmental sustainability.

EXPERIMENTAL

Materials

Acrylonitrile-butadiene-styrene ABS (grade 730) was procured from Shanghai Kingfa Technology Co., Ltd. Decabromodiphenyl ethane (DBDPE) was supplied by Shandong Haiwang Chemical Co., Ltd. Antimony trioxide (ATO) was sourced from Changde Chenzhou Antimony Co., Ltd. Ferric nitrate nonahydrate ($Fe(NO_3)_3{\cdot}9H_2O$) and zinc sulfate heptahydrate ($ZnSO_4{\cdot}7H_2O$) were obtained from Shanghai Macklin Biochemical Co., Ltd. Acrylonitrile butadiene rubber (NBR) was purchased from Rajchem (Mumbai, India). Deionized water was prepared in the laboratory.

Synthesis of Zinc Ferrite (ZF) Nanoparticles

The ZF nanoparticles were synthesized using a co-precipitation method. $ZnSO_4{\cdot}7H_2O$ and $Fe(NO_3)_3{\cdot}9H_2O$ were mixed at a molar ratio of 1:2 and dissolved in 200 mL of deionized water. The mixture was magnetically stirred at room temperature for 30 min until complete dissolution. Aqueous NaOH was then added dropwise to adjust the pH to 12 and stirring was continued. After reacting at 80 °C for 2 h, a ZF precursor was obtained. The precipitate was washed thoroughly with deionized water and absolute ethanol and then dried at 80 °C for 12 h to yield a reddish-brown intermediate (denoted as W-ZF). Finally, the W-ZF was calcined at 400 °C for 4 h in a muffle furnace to obtain the final ZF nanoparticles with an approximate yield of 90%. The overall synthetic process is illustrated in Fig. 1.

Preparation of ABS Composites

All samples were fabricated according to the formula in Table 1. Before compounding, the ABS and flame retardants were dried in a vacuum oven at 70 °C for 4 h. The dried raw materials were premixed in a high-speed mixer for 5 min according to the designed formulations, and then melt-blended with ABS using an RM-200C torque rheometer (Harbin Hapu Electric Technology Co., Ltd.) at 180 °C and 50 r/min. The prepared blends were compression-molded at 180 °C using a ZS-4063 flat vulcanizing machine (Dongguan Zhuosheng Mechanical Equipment Co., Ltd. Dongguan, China) to obtain standard samples for subsequent tests.

Characterization

Fourier transform infrared (FTIR) spectroscopy was performed using a Nicolet IS 5 spectrometer by scanning 32 times in the range of 4000–500 cm^{-1}.

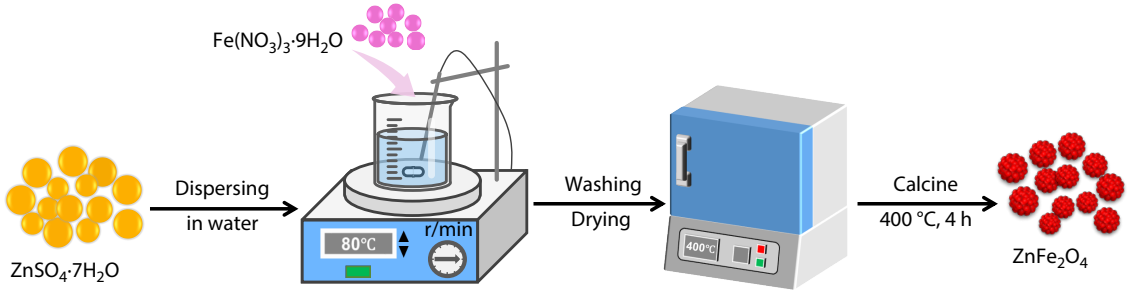

Fig. 1 Synthesis process of ZF nanoparticles.

X-ray powder diffraction (XRD) patterns were obtained using an X' Pert Pro diffractometer (Cu Kα radiation, λ=0.15418 nm; voltage: 40 kV, current: 40 mA).

Thermogravimetric analysis (TGA) was carried out on a TGA Q500 instrument (TA Co., USA), where approximately 5 mg of the sample was heated from 30 °C to 800 °C at a rate of 10 °C/min under nitrogen flow.

The limiting oxygen index (LOI) was measured according to ISO 4589-2 using a JF-3 oxygen index instrument (Nanjing Jiangning Instrument Factory, China), with a sample size of 100.0 mm × 6.5 mm× 3.2 mm.

The UL-94 vertical burning test was conducted using a JF-3 flame test apparatus (Jiangning Analytical Instrument Co., Ltd., China) in accordance with ISO 9773, with sample dimensions of 100.0 mm× 13.0 mm × 3.2 mm. Five samples were tested per group.

Cone calorimetry (CONE) testing was performed on a 100.0 mm × 100.0 mm × 3.2 mm sample using an FTT cone calorimeter under a heat flux of 50 kW/m^2.

Notched Izod impact tests were conducted on an XJJ-5 impact tester (JinJian Testing Instrument Co., Ltd., China) according to ASTM D256, with sample dimensions of 63.5 mm × 12.7 mm× 3.2 mm, and a notch radius of 45°. The average energy absorption was calculated for the five samples.

Tensile tests were performed using an XXJ-5 universal testing machine (JinJian Testing Co., Ltd., China) with a Type 1BA dumbbell-shaped sample with a total length of 75 mm, thickness of 2.0 mm, and gauge length of 25 mm. The samples were tested at a speed of 10 mm/min, and five samples were used to determine the average value.

The microstructure was observed using a HITACHI S4700 scanning electron microscope (SEM) at an acceleration voltage of 20 kV.

RESULTS AND DISCUSSION

Synthesis and Characterization of the ZF and W-ZF

The FITR spectra of the W-ZF and ZF are shown in Fig. 2(a). The ZF sample exhibited Zn—O and Fe—O bond peaks in the range of 400–600 cm^{-1}, which is a common feature of spinel ferrites. These correspond to the stretching vibrations of the octahedral and tetrahedral components of spinel ferrites.[25,26] As shown in Fig. 2(b), a comparison of the XRD patterns of ZF and W-ZF further confirmed the successful formation of W-ZF. ZF exhibits distinct diffraction peaks at 2θ values of 30.1°, 35.3°, 43.0°, 53.5°, 56.3°, and 62.4°, corresponding to the (220), (311), (400), (422), (511), and (440) planes of a cubic spinel structure (JCPDS No. 22-1012),[27–29] thereby verifying the successful formation of ZF.

The applicability of additives to melt-processed polymers is largely governed by their thermal stability under high-temperature extrusion and molding conditions. Therefore, TGA was conducted to evaluate the thermal degradation behavior of the ZF and its precursors. As shown in Fig. 2(c), the initial decomposition temperature ($T_{5\%}$) of ZF reaches 443.2 °C. These results demonstrate that, following hydrothermal synthesis and calcination, ZF derived from relatively unstable precursors exhibits remarkable thermal stability, thereby enabling its reliable application in the melt processing of most conventional polymers. Moreover, the prominent high char residue of ZF throughout the entire thermal degradation process reflects its excellent structural stability during decomposition.

Thermal Stability of ABS Composites

Thermogravimetric analyses of ABS and its composites under N_2 atmosphere are shown in Fig. 3, and the corresponding data are shown in Table 2. ABS undergoes a single-step decomposition, leaving a residue of 1.1%, which indicates its lack of charring ability. In contrast, ABS/12DBDPE/2ATO/2ZF and ABS/12DBDPE/2ATO/2ZF/5NBR showed a notable increase in residue from 1.1% to 7.1% and 14.7%, respectively. This enhancement reveals that the partial incorporation of ZF acts synergistically with the bromine-antimony system. The synergy originates from the ability of ZF to form a protective barrier in the condensed phase, which complements the gas-phase flame inhibition of the bromine-antimony system, thereby leading to more efficient char formation and a higher residue yield. The single peak in the

Table 1 The formulation of ABS composites.

Sample	ABS content (wt%)	DBDPE content (wt%)	ATO content (wt%)	ZF content (wt%)	NBR content (wt%)
ABS	100	–	–	–	–
ABS/12DBDPE/4ATO	84	12	4	–	–
ABS/12DBDPE/2ATO/2ZF	84	12	2	2	–
ABS/12DBDPE/2ATO/2ZF/5NBR	79	12	2	2	5

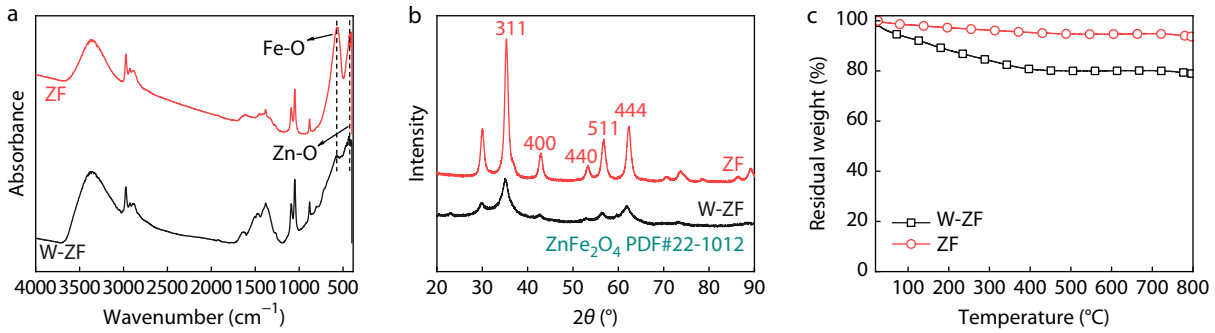

Fig. 2 Structural characterization of W-ZF and ZF: (a) FTIR spectra; (b) XRD patterns; (c) TGA curves.

DTG curve arises from the overlapping decomposition processes of the styrene-acrylonitrile (SAN) copolymer and butadiene rubber, as their decomposition temperatures are very close.

In contrast to ABS, the DTG curves of the binary (DBDPE/ATO), ternary (DBDPE/ATO/ZF), and quaternary (DBDPE/ATO/ZF/NBR) specimens exhibited two distinct peaks in similar temperature ranges. The first degradation peak for these systems appeared at a significantly lower temperature, and the second peak was similar to that of ABS. The $T_{5\%}$ and maximum mass loss temperature (T_{max}) of ABS were 384.2 and 425.3 °C, respectively. The incorporation of the DBDPE/ATO flame-retardant system significantly influenced the thermal degradation behavior of ABS. The $T_{5\%}$ for the ABS/12DBDPE/4ATO composite was 320 °C, which was approximately 64 °C lower than that of ABS. In addition, the DTG curves reveal a two-stage degradation process. The first peak corresponded to the decomposition of DBDPE and ATO, where the synergist ATO facilitated bromine release by gener-

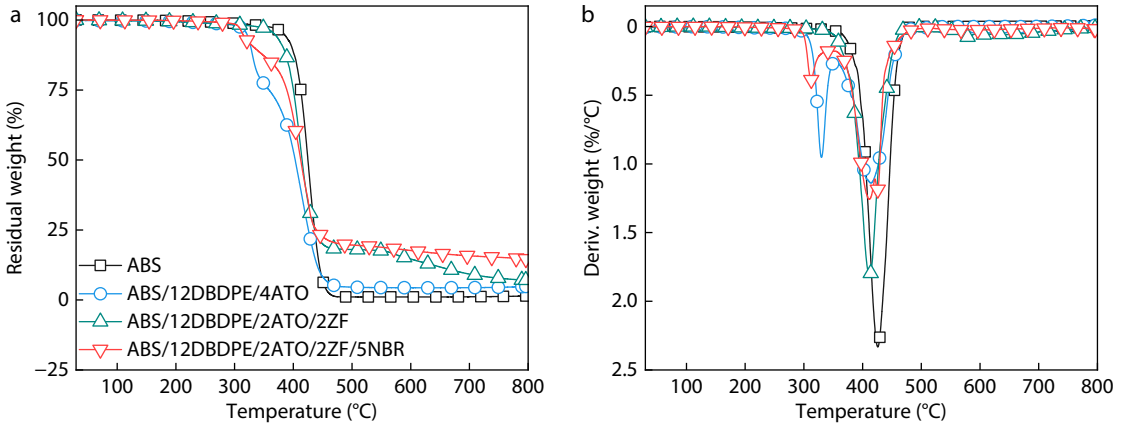

Fig. 3 (a) TGA and (b) DTG curves of different ABS composites.

Table 2 TGA data of ABS composites.

Sample	$T_{5\%}$ (°C)	T_{max} (°C)	Char yields at 800 °C (wt%)
ABS	384.0	425.3	1.1
ABS/12DBDPE/4ATO	320.8	415.1	4.8
ABS/12DBDPE/2ATO/2ZF	317.5	410.3	9.9
ABS/12DBDPE/2ATO/2ZF/5NBR	313.9	417.2	14.7

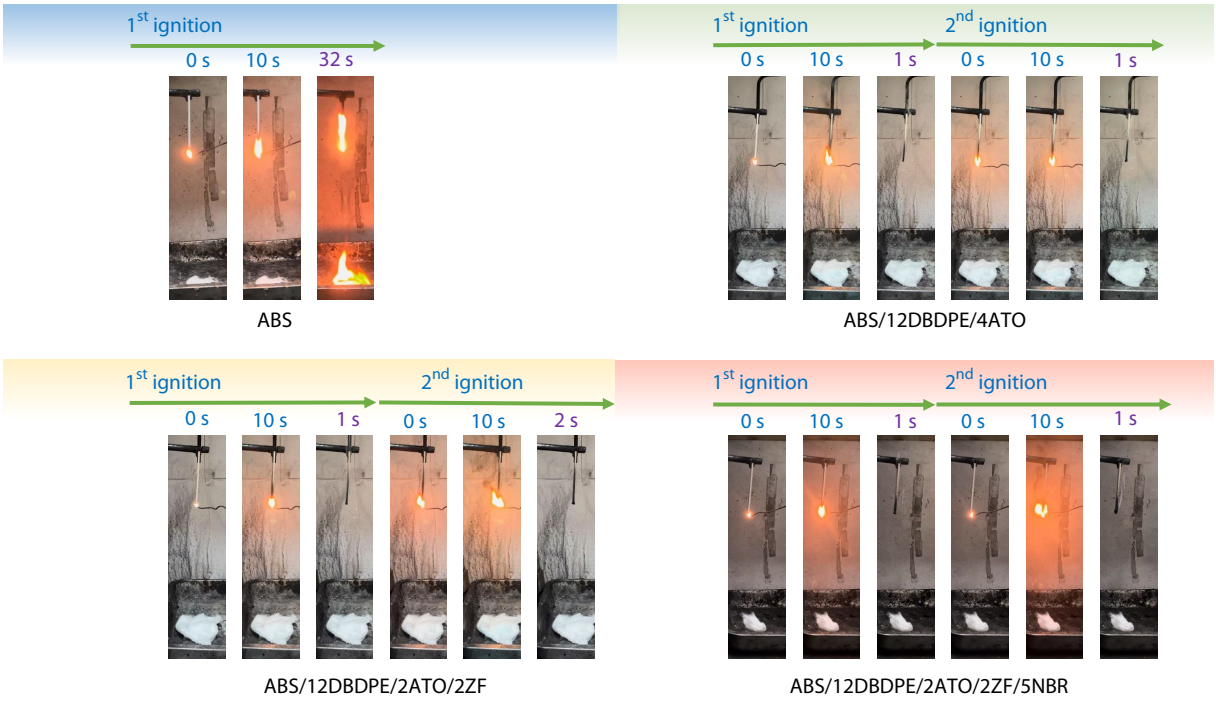

Fig. 4 Digital photographs of the UL-94 vertical burning test for ABS composites.

ating $SbBr_3$. The second decomposition peak was attributed to the thermal degradation of the ABS main chain. Compared to ABS/12DBDPE/4ATO, the char residue of the ABS/12DBDPE/2ATO/2ZF composite increased from 4.8% to 9.9%, indicating that ZF primarily acts in the condensed phase. For the ABS/12DBDPE/2ATO/2ZF/5NBR composite, the addition of NBR further increased the char residue content to 14.7% at 800 °C.

Flame Retardancy of ABS Composites

The flame retardancy of the composites was evaluated using LOI and UL-94 tests, and the corresponding results are presented in Fig. 4 and Table 3. As expected, ABS exhibited a low LOI value of 18%, failed to self-extinguish upon ignition, and burned completely with severe melt dripping that ignited the absorbent cotton during the UL-94 test. Incorporation of flame retardants markedly improved the performance: ABS/12DBDPE/4ATO showed an enhanced LOI of 24% and self-extinguishing after two ignitions, achieving a UL-94 V-0 rating. When 50 wt% ATO was replaced by ZF, ABS/12DBDPE/2ATO/2ZF increased the LOI to 27.1% while still attaining the V-0 rating. Furthermore, with the addition of 5 wt% NBR, ABS/12DBDPE/2ATO/2ZF/5NBR exhibited an LOI of 26.9% and retained the UL-94 V-0 rating, indicating that NBR does not compromise the beneficial effect of ZF replacement, and that the composite preserves excellent flame retardancy.

Cone calorimetry testing was performed to evaluate the combustion behavior of the ABS composites under realistic fire conditions.[30] The test yielded critical parameters, including the heat release rate (HRR), total heat release (THR), CO_2 production (CO_2P), residual mass (Mass), and fire performance index (FPI), as shown in Fig. 5 and Table 4.

Fire intensity is typically characterized by the peak heat release rate (PHRR). A higher PHRR denotes a more intense and rapid heat release, which accelerates the fire propagation and reduces the available escape and rescue times. As shown in Fig. 5(a), the ABS exhibited a PHRR of 940.3 kW/m^2. The incorporation of DBDPE and ATO markedly reduced the heat release. The ABS/12DBDPE/4ATO sample displayed a PHRR of 378.3 kW/m^2, which is 59.8% lower than that of ABS. When 50 wt% ATO was replaced by ZF, the PHRR of the ABS/12DBDPE/2ATO/2ZF sample further decreased to 356.6 kW/m^2. This improvement can be ascribed to the catalytic effect of ZF, which promotes early stage crosslinking of the ABS matrix, thereby generating a denser, more thermally stable char layer that effectively insulates the substrate and impedes oxygen diffu-

Table 3 LOI and UL-94 data for ABS composites.

Sample	LOI (%)	UL94			
		t_1 (s)	t_2 (s)	Dripping	Rating
ABS	18.0±0.2	>40	–	Y.	N.R.
ABS/12DBDPE/4ATO	24.0±0.1	1	1	N.	V-0
ABS/12DBDPE/2ATO/2ZF	27.1±0.3	1	2	N.	V-0
ABS/12DBDPE/2ATO/2ZF/5NBR	26.9±0.1	1	1	N.	V-0

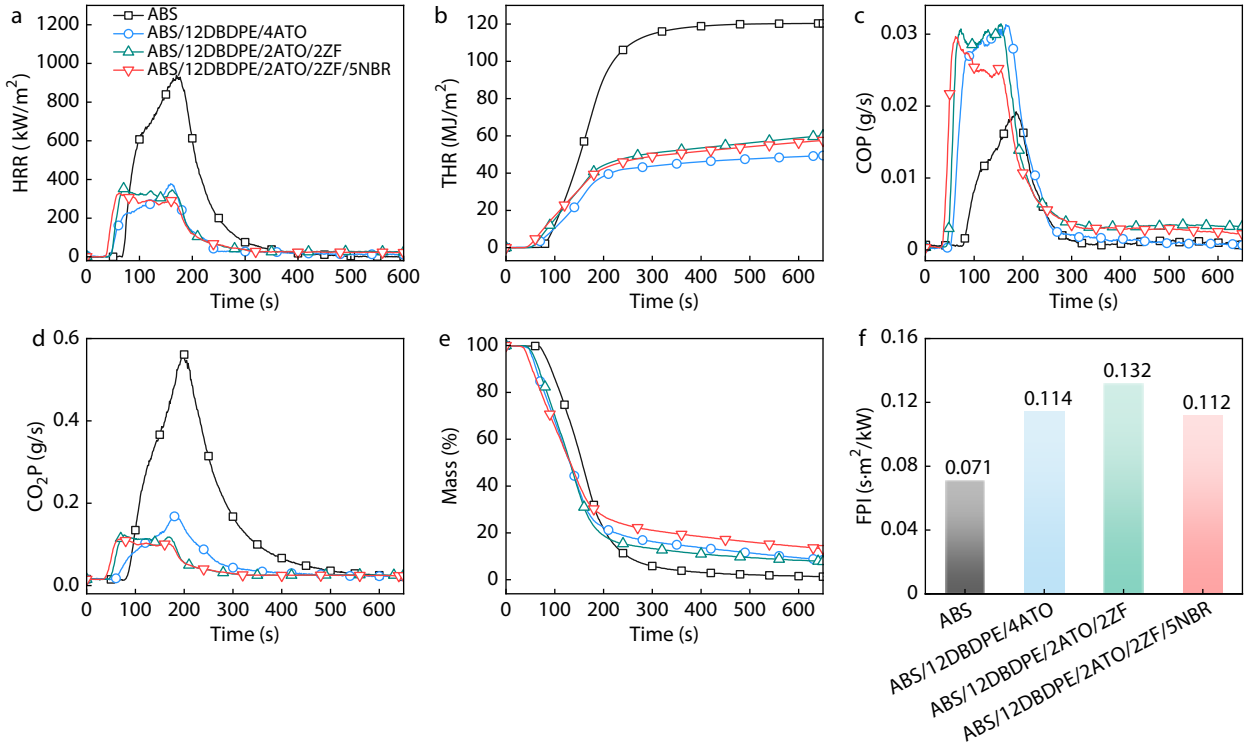

Fig. 5 Cone calorimetry data curves for ABS composites: (a) HRR, (b) THR, (c) COP, (d) Mass, (e) CO_2 Production, and (f) FPI.

https://doi.org/10.1007/s10118-026-3737-z

sion.[31]

The fire performance index (FPI, defined as TTI/PHRR) is widely used as a key indicator for evaluating the fire safety of polymer materials, with a higher FPI generally corresponding to a better flame-retardant efficiency.[32,33] Compared with the FPI of neat ABS (0.071 s·m^2/kW), the ABS/12DBDPE/2ATO/2ZF composite exhibited a significantly higher value of 0.132 s·m^2/kW. This result further demonstrates that the introduction of the 12DBDPE/2ATO/2ZF system substantially enhanced the flame retardancy of ABS.

Char Residue Analysis

It is well recognized that the morphology of protective char plays a crucial role in determining the condensed-phase flame-retardant mechanism. A continuous, tightly bonded, and thermally stable char layer is beneficial for enhancing the flame retardancy of the polymer matrix. As shown in Fig. 6(a), ABS was almost completely combusted during the cone calorimeter test, leaving only a small, fragmented residual evidence of rapid thermal degradation and high flammability at elevated temperatures.[34] For the ABS/12DBDPE/4ATO composite, the halogenated flame retardant mainly acted in the gas phase. Although it is effective at stopping flame reactions, this mechanism does not help form a strong and continuous protective char layer (Fig. 6b). Consequently, burning produces a large central cavity that fails to provide an effective char barrier to shield the underlying polymer.[35] However, with the incorporation of ZF, the ABS/12DBDPE/2ATO/2ZF composite formed a dense and continuous char layer on the surface after combustion (Fig. 6c). This residue effectively insulates against heat and restricts oxygen diffusion, indicating a dominant condensed-phase flame-retardant mechanism, and demonstrates that ZF promotes catalytic char formation.[31] The synergistic effect was further enhanced by adding NBR as an additional carbon source, which increased the char yield and produced a thicker, more coherent residue (Fig. 6d). Consequently, the flame retardancy of the ABS composites was markedly improved, primarily because of the enhanced char-forming capability of the condensed phase.[36]

Analysis of Flame Retardant Mechanisms

To further understand the synergistic interactions among the flame retardants, the chemical compositions of the char residues formed at different temperatures were systematically investigated using FTIR spectroscopy, as shown in Fig. 7. It can be observed that, in the temperature range from 350 °C to 450

Table 4 Cone calorimetry data for ABS composites.

Sample	THR (MJ/m^2)	PHRR (kW/m^2)	FPI (s·m^2/kW)	Residue (%)
ABS	120.4±2.1	940.3±5.1	0.071	1.3±0.2
ABS/12DBDPE/4ATO	49.7±3.5	378.3±4.2	0.114	5.3±0.3
ABS/12DBDPE/2ATO/2ZF	64.6±4.2	356.6±3.6	0.132	7.7±0.2
ABS/12DBDPE/2ATO/2ZF/5NBR	61.5±2.5	330.3±3.7	0.112	10.0±0.5

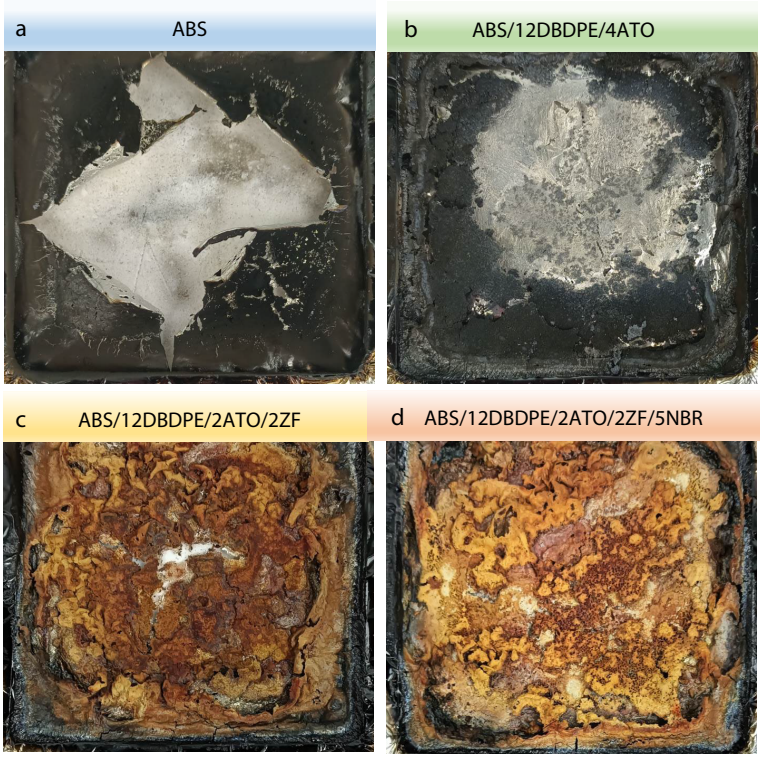

Fig. 6 Digital photos of samples after cone calorimeter tests. (a) ABS; (b) ABS/12DBDPE/4ATO; (c) ABS/12DBDPE/2ATO/2ZF; (d) ABS/12DBDPE/2ATO/2ZF/5NBR.

℃, the stretching vibration bands of ABS observed at 3067 and 3025 cm^{-1} (=C—H) and at 2917 and 2848 cm^{-1} (C—H) can be attributed to aromatic and aliphatic hydrocarbons originating from the thermal scission of styrene and butadiene chains, respectively. The absorption band at 2217 cm^{-1} was assigned to the C≡N stretching vibration of the acrylonitrile unit, which is one of the most characteristic absorption peaks of ABS.[37] Notably, this C≡N absorption band almost completely disappeared at temperatures above 500 ℃. The bands located at 1597, 1493, and 1452 cm^{-1} are attributed to the C=C skeletal vibrations and C—H bending vibrations of the benzene ring in the styrene units, indicating that the aromatic ring structure is gradually destroyed during thermal degradation. The absorption band at 749 cm^{-1} corresponds to the out-of-plane bending vibration of mono-substituted aromatic C—H. In the temperature range 500–600 ℃, most of the aforementioned absorption bands nearly vanish. Although the mono-substituted aromatic C—H absorption band at approximately 758 cm^{-1} could still be detected, its intensity gradually decreased, suggesting that the polymer main chains were completely decomposed.[38]

As shown in Fig. 7(b), the FTIR spectra of ABS/12DBDPE/4ATO exhibit absorption features nearly identical to those of ABS, suggesting that the Br-Sb flame-retardant system primarily operates in the gas phase and contributes negligibly to char formation in the condensed phase. In contrast, as shown in Fig. 7(c), ABS/12DBDPE/2ATO/2ZF exhibited a pronounced attenuation of the C—H stretching vibrations near 3000 cm^{-1} and a concurrent enhancement of the aromatic C=C absorption around 1500 cm^{-1} with increasing temperature, indicating that intensified dehydrogenation and aromatization are conducive to the formation of a dense and stable char layer.[39] The appearance of Zn-O and Fe-O absorption bands indicated the formation of a thermally stable inorganic network that cooperated with the carbonaceous char to construct an effective protective layer.[31] These results demonstrate that the incorporation of ZF effectively promotes condensed-phase char formation, thereby enhancing the flame-retardant performance of the composites.

Based on the above analysis, Fig. 8 schematically illustrates the proposed flame-retardancy mechanism of ABS composites. During combustion, a pronounced synergistic effect was observed in both the condensed and gaseous phases. In the condensed phase, ZF thermally decomposes to generate ZnO and Fe_2O_3.[31] These metal oxides, together with residual ZF, act as effective catalysts for carbonization, promoting the formation of a compact and thermally stable char layer. This char layer functioned as a physical barrier that restricted heat transfer and impeded the diffusion of oxygen and volatile degradation products to the underlying matrix.[40,41] Meanwhile, gas-phase flame-retardant activity was triggered simul-

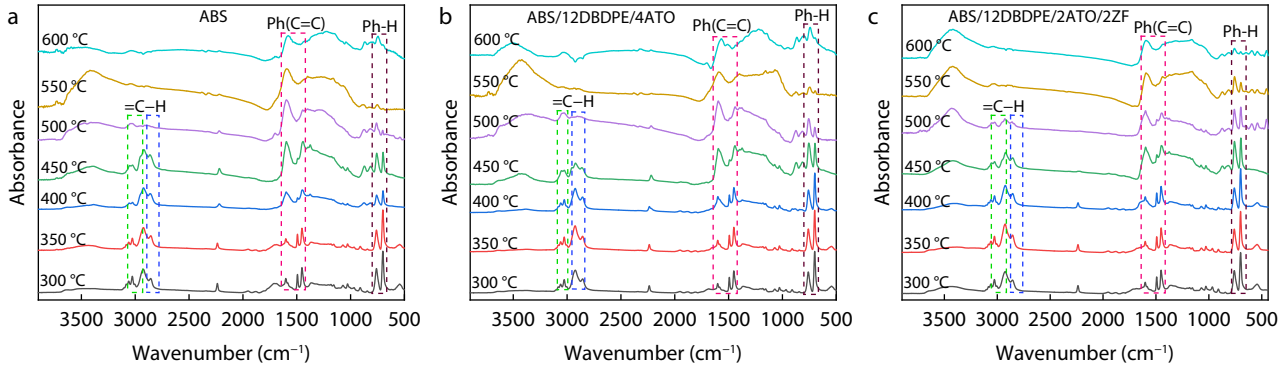

Fig. 7 FTIR spectra of char residues obtained from calcination at different temperatures: (a) ABS, (b) ABS/12DBDPE/4ATO, (c) ABS/12DBDPE/2ATO/2ZF.

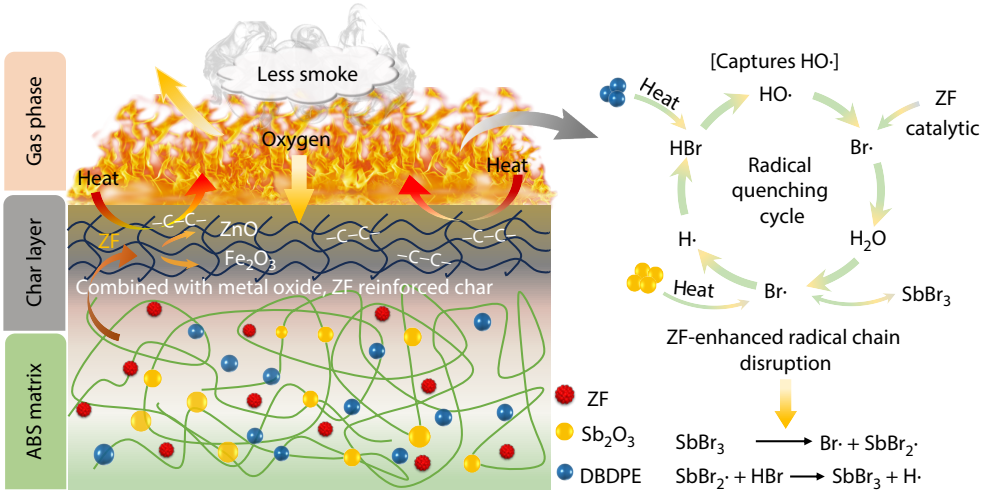

Fig. 8 Schematic diagram of the flame retardant mechanism in ABS/12DBDPE/2ATO/2ZF composite.

https://doi.org/10.1007/s10118-026-3737-z

taneously. Upon heating, DBDPE decomposed to release HBr and Br·. The released HBr reacts with ATO to form $SbBr_3$, which subsequently volatilizes and decomposes at elevated temperatures to generate additional Br·.[42] These radicals effectively scavenge H· in the flame zone, thereby disrupting the radical chain reactions responsible for flame propagation. In addition, HBr contributed to flame inhibition by diluting the local oxygen concentration and reacting with HO·, during which HBr was regenerated. This continuous radical quenching cycle further suppresses combustion.[43] Overall, the incorporation of ZF exhibited a pronounced synergistic interaction with the bromine-antimony flame-retardant system, leading to the formation of a reinforced char structure and enhanced gas-phase radical inhibition, which collectively accounted for the significantly improved flame retardancy of the ABS composites.

Mechanical Properties of ABS Composites

Impact and tensile strength tests were performed on the ABS composites, and the results are presented in Fig. 9. The notched impact strength of ABS reaches 20.0 kJ/m^2, which can be attributed to its three-block copolymer structure, in which the butadiene phase contributes to excellent toughness and mechanical performance.[44] However, for the ABS/12DBDPE/4ATO and ABS/12DBDPE/2ATO/2ZF samples, the notched impact strength decreases significantly to 4.6 and 3.8 kJ/m^2, respectively. This deterioration was mainly attributed to the introduction of ZF and ATO, both of which are inorganic particles. Their incorporation leads to poor interfacial compatibility between the fillers and the ABS matrix, thereby increasing material brittleness.[45] In contrast, when 5 wt% NBR was incorporated into the ABS/12DBDPE/2ATO/2ZF composite, a pronounced toughening effect was achieved, and the notched impact strength increased from 3.8 kJ/m^2 (ABS/12DBDPE/2ATO/2ZF) to 13.2 kJ/m^2 (ABS/12DBDPE/2ATO/2ZF/5NBR). This enhancement is attributed to the rubber toughening mechanism, where the NBR particles undergo cavitation under impact, triggering shear yielding of the ABS matrix and facilitating energy dissipation *via* plastic deformation. Meanwhile, improved interfacial compatibility alleviates the stress concentration, leading to a transition from brittle to ductile fracture behavior, thereby significantly enhancing the impact toughness.

According to the tensile tests shown in Figs. 9(b) and 9(c),

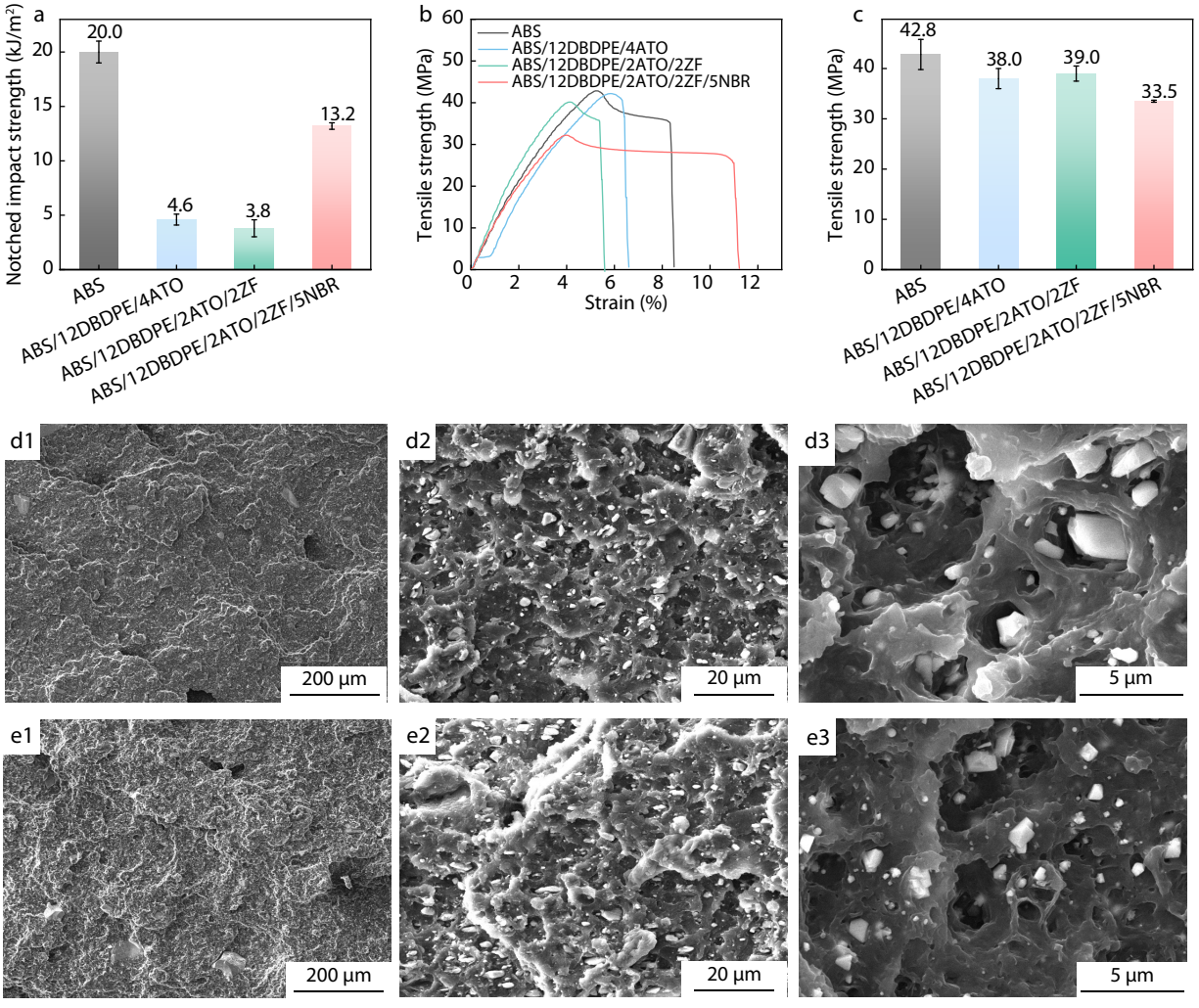

Fig. 9 (a) Notched impact strength, (b) tensile strength, (c) stress-strain curve and SEM micrographs of the fracture surface of impact sample: (d1–d3) ABS/12DBDPE/2ATO/2ZF and (e1–e3) ABS/12DBDPE/2ATO/2ZF/5NBR.

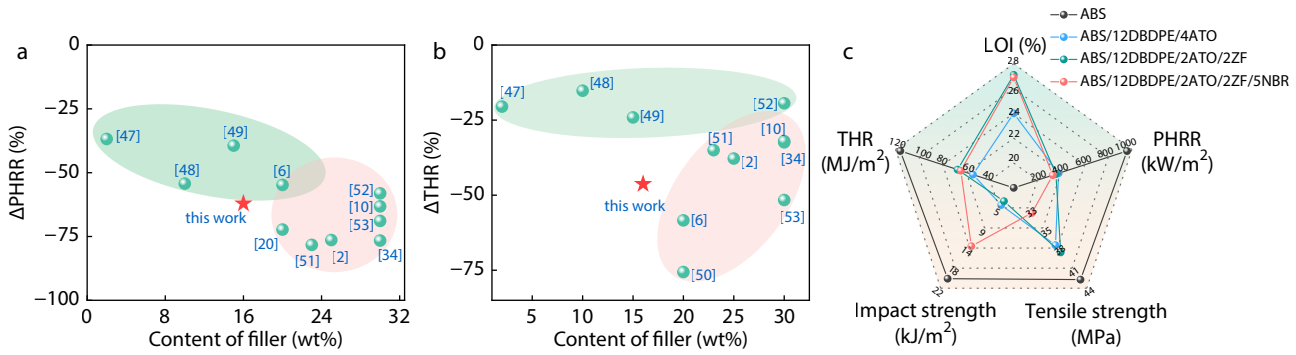

Fig. 10 (a) Radar plot comparing the properties of ABS composites; (b, c) Comparison of reduction of THR and PHRR between ABS/12DBDPE/2ATO/2ZF and other ABS blends or composites.

Table 5 Comprehensive performance comparison of different flame retardant systems that enable ABS to pass the UL94 V-0 rating.

Sample	Content (wt%)	LOI (%)	ΔPHRR (%)	ΔTHR (%)	Ref.
ABS/2Ag@PZS@MXene	2	24.0	36.8	20.5	[47]
ABS/10(Ce/P-CN)	10	28.6	54.0	15.2	[48]
ABS/15CM	15	/	39.4	24.1	[49]
ABS/20ADP@SiR	20	33.0	54.8	58.4	[6]
ABS/18IFR/2MIL-125	20	31.5	72.0	75.6	[50]
ABS/18DB–AO/5OMT	23	27.5	78.0	35.0	[51]
ABS/25MFAHP$_2$	25	26.0	76.4	37.8	[2]
ABS/30P-LIG	30	/	58.1	19.4	[52]
ABS/10LM/20IFR	30	27.2	63.3	32.0	[10]
ABS/2OLDH/28IFR	30	31.0	68.9	51.6	[53]
ABS/22.8Ce@APP/7.5DP	30	28.6	76.6	32.4	[34]
ABS/12DBDPE/2ATO/2ZF	16	27.1	62.1	46.3	This work

the tensile strengths of ABS, ABS/12DBDPE/4ATO, ABS/12DBDPE/2ATO/2ZF, and ABS/12DBDPE/2ATO/2ZF/5NBR composites were 42.8, 38.0, 39.0, and 33.5 MPa, respectively. The corresponding elongations at break are 8.4%, 6.6%, 5.6%, and 11.2%, respectively. Compared with neat ABS, the incorporation of inorganic particles reduced both the tensile strength and elongation at break of the material. However, after addition of NBR, the elongation at break increased by 33%.

The ABS composites showed no deterioration in impact performance either, as shown in Fig. 9(a). The fracture surfaces of the impact-tested specimens were examined using SEM. As shown in Figs. 9(d_1)–9(d_3), the impact fracture surface of the ABS/12DBDPE/2ATO/2ZF composite exhibited a noticeable agglomeration of inorganic particles. In particular, large voids can be observed in Fig. 9(d_3), which are attributed to the poor interfacial compatibility between the ABS matrix and inorganic fillers. The tendency of the fillers to aggregate leads to weak interfaces and localized stress concentration, ultimately resulting in a significant reduction in the impact strength.[2] In contrast, as shown in Figs. 9(e_1)–9(e_3), the ABS/12DBDPE/2ATO/2ZF/5NBR sample appears considerably rougher, with distinct stress-whitening evident. Under external loading, the NBR domains act as stress concentrators that effectively absorb the deformation energy, leading to pronounced stress whitening. Overall, the incorporation of NBR not only improved the interfacial compatibility between ABS and the inorganic particles, but also substantially enhanced the toughness of the composite.[46]

Properties Comparisons

In addition, the reduction in the PHRR and THR of the ABS/12DBDPE/2ATO/2ZF composite were compared with those of flame-retardant ABS systems reported in the literature, as summarized in Figs. 10(a), 10(b) and Table 5. ABS/12DBDPE/2ATO/2ZF exhibited pronounced decreases in PHRR and THR, reaching 62.1% and 46.3%, respectively, at a 50% replacement ratio of ATO. These reductions are superior to those achieved by the previously reported reference fillers (Fig. 10c), indicating that ZF can effectively function as an alternative synergist to ATO and offers a promising technical route for its partial substitution in flame-retardant ABS systems.

CONCLUSIONS

In this study, ZF nanoparticles were successfully synthesized *via* a co-precipitation method and employed as partial substitutes for ATO in flame-retardant ABS composites. When 50 wt% ATO was replaced by ZF, the resulting ABS/12DBDPE/2ATO/2ZF composite exhibited a significant improvement in flame retardancy, with the LOI increasing from 18% for ABS to 26.9% and achieving a UL-94 V-0 rating. In addition, compared with ABS/12DBDPE/4ATO, the ABS/12DBDPE/2ATO/2ZF composite exhibited a further decrease in the PHRR, demonstrating its superior flame-retardant efficiency. In addition to the improved fire performance, the partial substitution of ATO with ZF led to an estimated reduction in material cost. Furthermore, the incorporation of 5 wt% NBR as a toughening modifier effectively compensated for the loss in the impact resistance. The modified composite retained the UL-94 V-0 rating, whereas its impact strength increased by 247.4%. Overall, this work demonstrates that ZF is an effective and economical synergistic addi-

tive for brominated flame-retardant ABS systems and provides a cost-efficient and environmentally friendly strategy for partial replacement of ATO.

Conflict of Interests

The authors declare no interest conflict.

Data Availability Statement

The related data for this study are available from the corresponding authors upon reasonable request.

ACKNOWLEDGMENTS

This work was financially supported by the National Natural Science Foundation of China (Nos. 52573056 and 22475014).

REFERENCES

1 Xiong, L.; Huang, S. H.; Zhong, R. C.; Tang, W. Z.; Liu, C.; Jin, Y. Q. Preparation, characterization, and performance of lignin-based microencapsulated red phosphorus flame retardant for ABS. *J. Wuhan Univ. Technol.-Mat. Sci. Edit.* **2022**, *37*, 292–299.
2 Wu, N. J.; Xiu, Z. X.; Du, J. Y. Preparation of microencapsulated aluminum hypophosphite and flame retardancy and mechanical properties of flame-retardant ABS composites. *J. Appl. Polym. Sci.* **2017**, *134*, 14.
3 Sachdev, V. K.; Sharma, S. K.; Tomar, M.; Gupta, V.; Tandon, R. P. EMI shielding of MWCNT/ABS nanocomposites in contrast to graphite/ABS composites and MWCNT/PS nanocomposites. *RSC Adv.* **2016**, *6*, 45049–45058.
4 Chen, C. F.; Zhong, W. W.; Guo, J. H.; Liu, K.; Wang, A. D. Preparation and properties of ABS/BNNS composites with high thermal conductivity for FDM. *J. Polym. Eng.* **2023**, *43*, 875–883.
5 Abedini, A.; Asiyabi, T.; Campbell, H. R.; Hasanzadeh, R.; Azdast, T. On fabrication and characteristics of injection molded ABS/Al_2O_3 nanocomposites. *Int. J. Adv. Manuf. Technol.* **2019**, *102*, 1747–1758.
6 Zhou, F. S.; Tang, W.; Xi, W.; Qian, L. J.; Wang, J. Y.; Qiu, Y.; Chen, Y. J. Improving the fracture toughness, flame retardancy and smoke suppression of ABS by core-shell elastic flame retardant particles with P/Si synergistic effect. *Polym. Degrad. Stabil.* **2024**, *228*, 12.
7 Chen, S. J.; Chen, Z. R.; Bi, W. F.; Du, W.; Lin, L.; Hu, D. S.; Zhuo, H. T. Development of a Zr-based metal-organic framework (UiO-66) for a cooperative flame retardant in the PC/ABS. *Polymers* **2024**, *16*, 16.
8 Singh, R.; Prakash, S.; Kumar, V.; Pabla, B. S. 3D printed flame retardant, ABS-$C_4H_8N_6O$ composite as energy storage device. *Arab. J. Sci. Eng.* **2023**, *48*, 2995–3007.
9 Gao, Z. Y.; Zhu, Y.; Yuan, B. H.; Mu, B. Effect and mechanism study of mixed-dimensional palygorskite clay on thermo-stability, flame-retardant and smoke-suppression for PC/ABS composites. *J. Vinyl Addit. Technol.* **2024**, *30*, 1432–1445.
10 Wang, B. N.; Wu, B.; Zhang, G. S.; Yang, B. J. In-situ growth of layered double hydroxide on montmorillonite nanosheets to improve the flame retardant performance of ABS resin. *J. Vinyl Addit. Technol.* **2023**, *29*, 435–447.
11 Malinowski, R.; Krasinskyi, V.; Bajer, K.; Krasinska, O.; Augustyn, P.; Pietruszka, A.; Moraczewski, K. Utilization of wind turbine blade waste in the production of ABS composites and selected products based on these composites. *Polymers* **2025**, *17*, 18.
12 Yildiz, C.; Seki, Y.; Kizilkan, E.; Sarikanat, M.; Altay, L. Development of halogen-free flame retardant acrylonitrile butadiene styrene (ABS) based composite materials. *ChemistrySelect* **2023**, *8*, 11.
13 Zhang, J. F.; Hua, Y. F.; Liu, J.; Zhu, T.; Sun, J.; Gu, X. Y.; Li, H. F.; Zhao, J. M.; Zhang, S. Constructing flame retardant silica nanoparticles through styrene maleic anhydride copolymer

Graphical Abstract

Zinc Ferrite as an Eco-friendly Synergist for Decabromodiphenyl Ethane in Acrylonitrile Butadiene Styrene: an Effective Alternative to Antimony Trioxide for Enhanced Flame Retardancy

Ge-Hao Guo, Miao-Miao Tian, Meng-Yuan Zheng, Qing-Hua Peng, Xiang Tan, Chang-Hui Luo, Jun Sun, Xiao-Yu Gu, Hong-Fei Li, and Sheng Zhang

Beijing University of Chemical Technology

Partial replacement of antimony trioxide with zinc ferrite synergistically enhanced the flame retardancy of acrylonitrile butadiene styrene (ABS), while nitrile butadiene rubber improved impact strength without compromising flame retardancy.

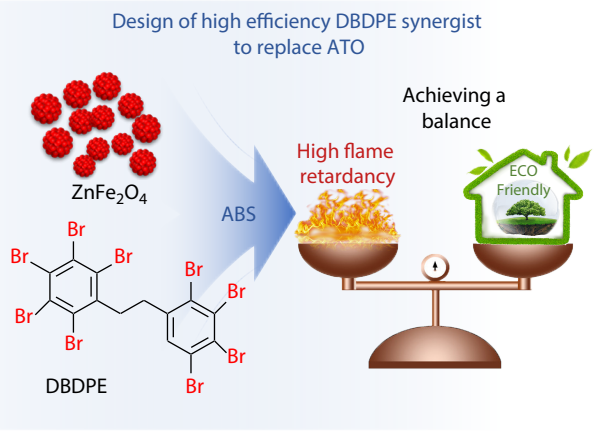

Chinese J. Polym. Sci., 2026 *https://doi.org/10.1007/s10118-026-3737-z*

grafting for PC/ABS composites. *Compos. Pt. A-Appl. Sci. Manuf.* **2023**, *175*, 10.
14 Rodriguez, A.; Herrero, M.; Asensio, M.; Santiago-Calvo, M.; Guerrero, J.; Cañibano, E.; Fernández, M. T.; Nuñez, K. Cooperative effect of chemical and physical processes for flame retardant additives in recycled ABS. *Polymers* **2023**, *15*, 17.
15 Chen, J.; Rong, L.; Fang, W.; Liu, J. Y.; Liu, X. Q. Highly efficient intumescent flame retardant coating for ABS: Preparation and application. *J. Appl. Polym. Sci.* **2022**, *139*, 9.
16 Li, M. D.; Nie, B.; Sun, L. T.; Cao, C. L.; Ma, J. Y. Enhancement of flame retardancy of ACS resin with synergistic flame retardant antimony oxide/decabromodiphenyl ethane. *J. Macromol. Sci. Part A-Pure Appl. Chem.* **2025**, *62*, 285−293.
17 Schildroth, S.; Osborne, G.; Smith, A. R.; Yip, C.; Collins, C.; Smith, M. T.; Sandy, M. S.; Zhang, L. P. Occupational exposure to antimony trioxide: a risk assessment. *Occup. Environ. Med.* **2021**, *78*, 413−418.
18 Chen, X. R.; Birnbaum, L. S.; Babich, M. A.; de Boer, J.; White, K. W.; Barone, S., Jr.; Fehrenbacher, C.; Stapleton, H. M. Opportunities in assessing and regulating organohalogen flame retardants (OFRs) as a class in consumer products. *Environ. Health Perspect.* **2024**, *132*, 10.
19 Bevington, C.; Williams, A. J.; Guider, C.; Baker, N. C.; Meyer, B.; Babich, M. A.; Robinson, S.; Jones, A.; Phillips, K. A. Development of a flame retardant and an organohalogen flame retardant chemical inventory. *Sci. Data* **2022**, *9*, 10.
20 Cai, T. M.; Wang, J. L.; Zhang, C. H.; Cao, M.; Jiang, S. J.; Wang, X.; Wang, B. B.; Hu, W. Z.; Hu, Y. Halogen and halogen-free flame retarded biologically-based polyamide with markedly suppressed smoke and toxic gases releases. *Compos. Pt. B-Eng.* **2020**, *184*, 11.
21 Guo, L. C.; Lv, Z. L.; Zhu, T. T.; He, G. H.; Hu, J. X.; Xiao, J. P.; Liu, T.; Yu, S. B.; Zhang, J. L.; Zhang, H.; Ma, W. J. Associations between serum polychlorinated biphenyls, halogen flame retardants, and renal function indexes in residents of an e-waste recycling area. *Sci. Total Environ.* **2023**, *858*, 10.
22 Zhang, Y. S.; Qian, L. J.; Qu, L. J.; Wang, J. Y.; Qiu, Y.; Xi, W.; Ma, Y. Bismuth trioxide replaced diantimony trioxide to obtain polyvinyl chloride leather with high flame retardancy and low flame propagation rate. *React. Funct. Polym.* **2024**, *197*, 13.
23 Zhang, Y. S.; Qian, L. J.; Qu, L. J.; Wang, J. Y.; Qiu, Y.; Xi, W.; Ma, Y. Effect of partial replacement of antimony trioxide with zinc borate and stannic oxide on the flame retardancy of flexible PVC films. *J. Appl. Polym. Sci.* **2024**, *141*, 14.
24 Mao, N. D.; Thanh, T. D.; Thuong, N. T.; Grillet, A. C.; Kim, N. H.; Lee, J. H. Enhanced mechanical and thermal properties of recycled ABS/nitrile rubber/nanofil N15 nanocomposites. *Compos. Pt. B-Eng.* **2016**, *93*, 280−288.
25 Islam, S.; Rahman, M. L.; Moni, M. R.; Biswas, B.; Ahmed, M. F.; Sharmin, N. Impacts of annealing temperature on microstructure, optical and electromagnetic properties of zinc ferrites nanoparticles synthesized by polymer assisted sol-gel method. *Arab. J. Chem.* **2023**, *16*, 19.
26 Hassanzadeh-Afruzi, F.; Esmailzadeh, F.; Heidari, G.; Maleki, A.; Zare, E. N. Arabic gum-grafted-hydrolyzed polyacrylonitrile@$ZnFe_2O_4$ as a magnetic adsorbent for remediation of levofloxacin antibiotic from aqueous solutions. *ACS Omega* **2023**, *8*, 6337−6348.
27 Al-Wasidi, A. S.; Alreshaidan, S. Enhanced removal of rhodamine b dye from aqueous media *via* adsorption on facilely synthesized zinc ferrite nanoparticles. *Inorganics* **2024**, *12*, 26.
28 Sattar, A.; Bofeng, B.; Khalil, M.; Sajjad, M. Detailed analysis of structural, optical and photo catalytic properties of spinel nickel doped magnesium zinc ferrites at different substitutions. *Inorg. Chem. Commun.* **2022**, *142*, 10.
29 Xie, Z. Q.; Jiang, T.; Chen, F.; Guo, Y. F.; Wang, S.; Yang, L. Z. Phase transformation and zinc extraction from zinc ferrite by calcium roasting and ammonia leaching process. *Crystals* **2022**, *12*, 13.
30 Hermouet, F.; Rogaume, T.; Guillaume, E.; Richard, F.; Marquis, D.; Ponticq, X. Experimental characterization of the reaction-to-fire of an acrylonitrile-butadiene-styrene (ABS) material using controlled atmosphere cone calorimeter. *Fire Saf. J.* **2021**, *121*, 17.
31 Sun, X. M.; Li, Z. W.; Das, O.; Hedenqvist, M. S. Superior flame retardancy and smoke suppression of epoxy resins with zinc ferrite@polyphosphazene nanocomposites. *Compos. Pt. A-Appl. Sci. Manuf.* **2023**, *167*, 9.
32 Kim, M. H.; Seo, H. J.; Lee, S. K.; Lee, M. C. Influence of thermal aging on the combustion characteristics of cables in nuclear power plants. *Energies* **2021**, *14*, 17.
33 Zhou, X.; Qiu, S. L.; He, L. X.; Wang, X.; Zhu, Y. L.; Chu, F. K.; Wang, B. B.; Song, L.; Hu, Y. Synthesis of star-shaped allyl phosphazene small molecules for enhancing fire safety and toughness of high performance BMI resin. *Chem. Eng. J.* **2021**, *425*, 15.
34 Meng, P.; Xiao, H. R.; Zhang, F.; Jia, R. S.; Zhu, L. X.; Shao, Z. B. Green facile fabrication of halogen-free flame-retardant ABS with high mechanical performance. *RSC Adv.* **2025**, *15*, 19456−19467.
35 Nakashima, E.; Hosokawa, Y.; Ueno, T. Synergistic flame retardancy of solid acid, hindered N-alkoxy amine, and halogen compound for polypropylene. *J. Appl. Polym. Sci.* **2023**, *140*, e54511.
36 Hao, X.; Wang, G.; Wang, X.; Li, K.; He, Q. The thermal stability and flame retardant effect of $Al(OH)_3$ on NBR containing intumescent flame retardant. *J. Polym. Res.* **2023**, *30*, 410.
37 Huang, G. B.; Chen, W.; Wu, T.; Guo, H. C.; Fu, C. Y.; Xue, Y. J.; Wang, K.; Song, P. A. Multifunctional graphene-based nano-additives toward high-performance polymer nanocomposites with enhanced mechanical, thermal, flame retardancy and smoke suppressive properties. *Chem. Eng. J.* **2021**, *410*, 12.
38 Lin, Y. H.; Li, S. J.; Du, L.; Dong, W. H.; Chen, X. L.; Gao, Q. Y.; Wang, B. Interfacial engineering of 0D-2D hierarchical MXene@PEI@AgNC nanohybrids to achieve flame retardant, mechanical and antibacterial properties of ABS nanocomposites. *Chem. Eng. J.* **2024**, *499*, 15.
39 Jang, J.; Kim, J.; Bae, J. Y. Synergistic effect of ferric chloride and silicon mixtures on the thermal stabilization enhancement of ABS. *Polym. Degrad. Stabil.* **2005**, *90*, 508−514.
40 Wang, X. D.; Yin, Y. J.; Li, M. L.; Hu, Y. Hexagonal boron Nitride@$ZnFe_2O_4$ hybrid nanosheet: An ecofriendly flame retardant for polyvinyl alcohol. *J. Solid State Chem.* **2020**, *287*, 8.
41 Lyu, P.; Hou, Y. B.; Wang, R. Z.; Ma, M. L.; Chen, Y.; Xing, Q. Y.; Ma, Y.; Wang, S.; Wu, Y. F.; Huang, W. B. Synthesis of $ZnFe_2O_4$@Mg-Al-SDBS LDH composites for regulating heat and fire safety properties of polyurea. *Polym. Adv. Technol.* **2022**, *33*, 4290−4301.
42 Xu, J. L.; Liu, X. Q.; Yang, W. L.; Niu, L.; Zhao, J. Q.; Ma, B. X.; Kang, C. H. Influence of montmorillonite on the properties of halogen-antimony flame retardant polypropylene composites. *Polym. Compos.* **2019**, *40*, 1930−1938.
43 Cheng, C. Z.; Xu, Z. K.; Zhao, Q. B.; Gao, M.; Li, T.; Li, G. Z.; Chi, K. D.; Xu, J. G.; Cheng, B. W. Prepartion of low-cost blended lyocell fibres with phosphorus, nitrogen, halogen and inorganic flame retardants and study on their synergistic fame retardancy mechanism. *Int. J. Biol. Macromol.* **2024**, *282*, 11.
44 Nigam, I.; Nigam, D.; Mathur, G. N. Effect of rubber content of ABS on properties of PC/ABS blends. 1. Rheological, mechanical, and thermal properties. *Polym.-Plast. Technol. Eng.* **2005**, *44*, 815−832.
45 Xia, J.; Luo, X.; Huang, J.; Ma, J. J.; Yang, J. X. Preparation of core/shell organic-inorganic hybrid polymer nanoparticles and their application to toughening poly(methyl methacrylate). *RSC Adv.* **2021**, *11*, 34036−34047.

46 Zhang, J.; Wang, X.; Tan, L.; Wang, Q.; Yu, H.; Xu, W.; Xu, B.; Xiao, S.; Huang, J. A facile toughening strategy for styrene-acrylonitrile copolymer through dynamic vulcanization of acrylonitrile-butadiene rubber. *J. Appl. Polym. Sci.* **2026**, *143*, e57992.
47 Lin, Y. H.; Dong, W. H.; Li, S. J.; Zhang, S. H.; Chen, X. L.; Du, L.; Wang, B. Core-shell Ag@PZS modified MXene towards highly flame retardancy, electromagnetic interference shielding, antibacterial of robust tough hierarchical ABS composites. *Compos. Pt. A-Appl. Sci. Manuf.* **2025**, *192*, 14.
48 Huang, G. B.; Huo, S. Q.; Ren, J. H.; Chen, W.; Yang, H. Q.; Xiao, S. W.; Wang, T. L.; Peng, H.; Song, P. A. Engineering Ce/P-functionalized g-C_3N_4 for advanced ABS nanocomposites exhibiting unparalleled fire retardancy, enhanced thermal and mechanical properties. *Appl. Mater. Today* **2024**, *38*, 10.
49 Li, W. M.; Huang, G. B.; Chen, H. F.; Wang, T.; Yang, J. G.; Chen, W.; Wang, T. L. Cerium molybdate nanosheets as a multifunctional flame retardant for enhancing fire safety and mechanical strength of ABS composites. *Mater. Today Commun.* **2025**, *49*, 9.
50 Zhang, Z. R.; Quan, Y. F.; Shen, R. Q.; Wang, K. Y.; Zhou, H. C.; Wang, Q. S. Synergistic effects of titanium-based MOFs MIL-125 with intumescent flame retardants in ABS polymer composites on flame retardancy study. *Fire-Switzerland* **2024**, *7*, 17.
51 Wang, S. F.; Hu, Y.; Zong, R. W.; Tang, Y.; Chen, Z. Y.; Fan, W. C. Preparation and characterization of flame retardant ABS/montmorillonite nanocomposite. *Appl. Clay Sci.* **2004**, *25*, 49–55.
52 Prieur, B.; Meub, M.; Wittemann, M.; Klein, R.; Bellayer, S.; Fontaine, G.; Bourbigot, S. Phosphorylation of lignin to flame retard acrylonitrile butadiene styrene (ABS). *Polym. Degrad. Stabil.* **2016**, *127*, 32–43.
53 Hu, D. T.; Zhou, Q. Q.; Zhou, K. Q. Combined effects of layered nanofillers and intumescent flame retardant on thermal and fire behavior of ABS resin. *J. Appl. Polym. Sci.* **2019**, *136*, 11.

https://doi.org/10.1007/s10118-026-3737-z